

DRIFT ORBITS OF ENERGETIC PARTICLES IN AN INTERPLANETARY MAGNETIC FLUX ROPE

W. KRITTINATHAM^{1,2} AND D. RUFFOLO^{1,2}

¹ Department of Physics, Faculty of Science, Mahidol University, Rama VI Road, Bangkok 10400, Thailand; watcharawuth.krittinatham@gmail.com, scdjr@mahidol.ac.th

² ThEP Center, CHE, 328 Si Ayutthaya Road, Bangkok 10400, Thailand

Received 2009 April 26; accepted 2009 August 31; published 2009 September 25

ABSTRACT

Interplanetary magnetic flux ropes have significant effects on the distribution of energetic particles in space. Flux ropes can confine solar energetic particles (SEPs) for hours, and have relatively low densities of Galactic cosmic rays (GCRs), as seen during second-stage Forbush decreases. As particle diffusion is apparently inhibited across the flux rope boundary, we suggest that guiding center drifts could play a significant role in particle motion into and out of the flux ropes. We develop an analytic model of the magnetic field in an interplanetary magnetic flux rope attached to the Sun at both ends, in quasi-toroidal coordinates, with the realistic features of a flux rope cross section that is small near the Sun, expanding with distance from the Sun, and field lines that are wound less tightly close to the Sun due to stretching by the solar wind. We calculate the particle drift velocity field due to the magnetic field curvature and gradient as a function of position and pitch-angle cosine, and trace particle guiding center orbits numerically, assuming conservation of the first adiabatic invariant. We find that SEPs in the interior of a flux rope can have drift orbits that are trapped for long times, as in a tokamak configuration, with resonant escape features as a function of the winding number. For Forbush decreases of GCRs, the drifts should contribute to a unidirectional anisotropy and net flow from one leg of the loop to the other, in a direction determined by the poloidal field direction.

Key words: cosmic rays – solar–terrestrial relations – Sun: coronal mass ejections (CMEs) – Sun: magnetic fields

1. INTRODUCTION

Coronal mass ejections (CMEs), transient events in which magnetized plasma is ejected from the Sun (Tousey 1973), can often drag solar magnetic flux ropes into the interplanetary medium to the Earth and beyond, even to the outer heliosphere (Burlaga et al. 1981b; Burlaga 1995). The scientific interest in such interplanetary magnetic flux ropes and associated CME plasma focuses on their magnetic topology, often with field lines helically wrapped around a curved central axis (Burlaga et al. 1981b), their frequent association with distinctive plasma properties (see Gosling 1990, and references therein), their disturbance of the interplanetary medium and shock formation (e.g., Burlaga et al. 1981b; Gosling & McComas 1987; Manchester et al. 2004), and impacts of the shocks and strong magnetic fields on the Earth’s magnetosphere, leading to geomagnetic storms (e.g., Gonzalez & Tsurutani 1987; Marubashi 2000), which are also of practical interest for their space weather effects on human activities.

Another aspect of space weather is the prompt arrival of solar energetic particles (SEPs) to near-Earth space. Of particular interest are ground level enhancements (GLEs), i.e., events in which the flux of relativistic SEP ions of energy $\gtrsim 1$ GeV nucleon $^{-1}$ is so high that there is a measurable enhancement over the ambient Galactic cosmic ray (GCR) flux (Forbush 1946; Meyer et al. 1956). These relativistic solar particles, as well as subrelativistic SEPs that arrive as a strong, prompt pulse, are associated with space weather effects such as satellite failures and radiation hazards to astronauts and air crews (Wilson et al. 2003). These SEPs can be accelerated either by impulsive solar flares or by CME-driven shocks, with the latter providing a more intense flux (Reames 1999).

The most intense and energetic beams of SEPs (such as those during GLEs) are produced over short time durations (Bieber et al. 2002, 2004, 2005; Ruffolo et al. 2006), with injection start times that are consistent with acceleration at a

CME shock while it was close to the Sun (Kahler 1994; Tylka et al. 2003; Bieber et al. 2004, 2005; Gopalswamy et al. 2005; Reames 2009). Because major solar events frequently occur in a sequence of several events from the same solar active region, it is not uncommon for SEPs to be injected into an interplanetary medium that was disturbed due to a preceding CME (Bieber et al. 2002).

Recently, particular interest has focused on transport effects on the temporal evolution and directional distribution of SEPs injected inside an interplanetary magnetic flux rope due to a preceding CME (Torsti et al. 2004; Kocharov et al. 2005, 2007; Bieber et al. 2005; Miroshnichenko et al. 2005; Ruffolo et al. 2006; Sáiz et al. 2008), as shown schematically in Figure 1. Interplanetary magnetic flux ropes are associated with low magnetic fluctuations and weak pitch-angle scattering of particles (Burlaga et al. 1981a; Tranquille et al. 1987), so they provide an interplanetary “highway” for SEPs to arrive as an intense beam (Torsti et al. 2004). Even after the weak pitch-angle scattering eventually spreads out the directional distribution, these particles can be trapped for extended periods by the closed magnetic field lines. For example, during the GLE of 1989 October 22, the propagation of SEPs inside a flux rope led to an intense, beam-like pulse of particles immediately after the solar event, and at long times the relativistic solar particle intensity was unusually persistent, with an exponential decay over 3 hr (Ruffolo et al. 2006). These features of propagation inside a flux rope have implications for the space weather effects of SEPs.

Another example of the effects of an interplanetary magnetic flux rope on energetic particles is the second stage of a Forbush decrease in GCRs (Forbush 1937; Hess & Demmelmaier 1937). While the first stage begins as a CME-driven shock passes the detector, the second stage (if present) is associated with the passage of CME ejecta (Cane et al. 1996). The maximum decrease is up to $\sim 25\%$ at a rigidity of ≈ 1 GV. Bidirectional flows are frequently observed, which is evidence for the passage of a closed interplanetary magnetic flux rope (Richardson et al.

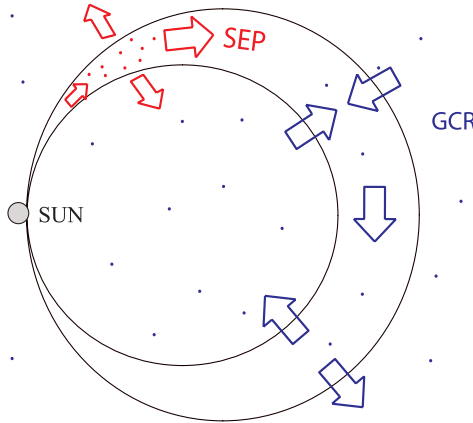


Figure 1. Illustration of the effect of an interplanetary magnetic flux rope (black) on energetic particles in space. The particles basically follow field lines, so their motion across magnetic flux surfaces is inhibited. Solar energetic particles (SEPs; red) can be trapped inside the flux rope for extended time periods. Galactic cosmic rays (GCRs; blue) have a lower density inside a flux rope, a phenomenon known as a Forbush decrease, in part because it is difficult for GCRs to enter the flux rope from outside. The present work considers the drift orbits of particles in the flux rope, and to what extent guiding center drifts allow particles to cross magnetic flux surfaces and enter or exit the flux rope. One of our results, schematically indicated here, is that drifts are predominantly inward along one leg of the loop and outward along the other, which should contribute to a unidirectional anisotropy and net flow of GCRs in one direction.

2000). Evidently, the particle density inside the loop is not in equilibrium with that outside, apparently because GCRs from outside cannot easily enter the flux rope, or require an extended timescale to do so.

Here, we address the mechanisms by which energetic particles can enter or exit an interplanetary magnetic flux rope, or conversely how SEPs can be trapped and the entrance of GCRs can be inhibited (see Figure 1). To enter or exit a closed magnetic field structure, particles must evidently cross magnetic field lines, either by gradient and curvature drifts, or by a particular type of diffusion in which particles no longer follow the same field line. To expand on this, we note that particle transport perpendicular to the large-scale field has two mutually interacting physical mechanisms: (1) particles follow turbulent field lines that undergo a random walk with respect to the large-scale field (Jokipii 1966), which eventually yields subdiffusion of particles in the perpendicular direction (Gremantsev 1963; Urch 1977; Kóta & Jokipii 2000); and (2) the particle motion ceases to be correlated with the direction of its original guiding field line, which yields diffusion at late times (Qin et al. 2002; Matthaeus et al. 2003; Ruffolo et al. 2008). The combination of these two processes is sometimes called “cross-field” transport, though it would be more accurate to reserve that term for mechanism 2. Mechanism 1 alone cannot explain how particles transfer between closed field lines in the flux rope and open field lines outside. This major component of perpendicular diffusion may be effective either inside or outside the flux rope, but not across the flux rope boundary, where truly cross-field transport is needed. Indeed, observations of both SEPs (e.g., Lario et al. 2004) and GCRs (e.g., Cane 2000) indicate particularly sharp gradients in particle density across the boundaries of flux ropes, supporting the idea that diffusion

is relatively ineffective at transferring particles across flux rope boundaries.

The relative ineffectiveness of perpendicular diffusion suggests that gradient and curvature drifts due to the large-scale magnetic field play a major role, or the dominant role, in particle transfer across the boundary of an interplanetary magnetic flux rope. Indeed, a proper understanding of particle transport inside the flux rope, especially over long timescales, requires an understanding of the drift motions, which to date have not been specifically examined for a realistic magnetic field model.

Therefore, the present work investigates the drift orbits of particles in a model interplanetary magnetic flux rope. To capture the essential large-scale properties of a flux rope and provide an easy prescription for the field gradient computations necessary to estimate the drifts, we develop a global analytic model of an interplanetary magnetic flux rope. We require the field winding to be tighter at the outermost portion of the flux rope, while the field lines are straighter near the Sun due to stretching by the solar wind. The cross-sectional area of the flux rope also depends on distance from the Sun, and should be proportional to distance squared at a small distance from the Sun, a feature that is crucial for proper magnetic mirroring of particles. We find that the winding of field lines in the flux rope inhibits the escape of SEPs from the inner portion, analogous to the well-known trapping of particles in tokamak experiments on magnetic confinement fusion (Tamm 1961a, 1961b; Sakharov 1961). However, in the outer portion of the flux rope, the drift orbits allow particles to enter or exit the flux rope. Interestingly, the particles should predominantly drift in along one leg of the rope and out along the other, contributing to a unidirectional flow and anisotropy.

2. BASIC REQUIREMENTS OF A FLUX ROPE MODEL

2.1. Lessons and Limitations of Simple Models

First, let us review what can be learned from the drift velocity of energetic particles in simple models of magnetic flux ropes, and why a more detailed model is required to capture the realistic features of drift orbits in interplanetary flux ropes.

Using μ as the cosine of the pitch angle, i.e., the angle between the particle velocity \mathbf{v} and the magnetic field, the gradient drift for a particle of mass m and charge q is given by

$$\mathbf{v}_g = \frac{\gamma m(1 - \mu^2)v^2}{2qB^3} \mathbf{B} \times \nabla B \quad (1)$$

and the curvature drift is

$$\mathbf{v}_c = \frac{\gamma m\mu^2 v^2}{qB^2} \mathbf{B} \times \boldsymbol{\kappa} = -\frac{\gamma m\mu^2 v^2}{qB^2} \mathbf{B} \times \frac{\mathbf{R}_c}{R_c^2}, \quad (2)$$

where $\gamma = (1 - v^2/c^2)^{-1/2}$, c is the speed of light, $\boldsymbol{\kappa}$ is the curvature, and \mathbf{R}_c is the radius of curvature of the field line, expressed as a vector outward from the center of curvature, satisfying

$$\boldsymbol{\kappa} = -\frac{\mathbf{R}_c}{R_c^2} = (\hat{\mathbf{b}} \cdot \nabla)\hat{\mathbf{b}}, \quad (3)$$

where $\hat{\mathbf{b}}$ is the unit vector along \mathbf{B} .

Interplanetary flux ropes have frequently been modeled as straight, cylindrical flux ropes. In cylindrical coordinates, the magnetic field varies only with distance ρ from the loop axis, and flux surfaces are cylinders of constant ρ . In this case, ∇B is

in the $\hat{\rho}$ direction, and from the cross-product in Equation (1), \mathbf{v}_g is then along the flux surface and perpendicular to \mathbf{B} . Similarly, \mathbf{R}_c is along $\hat{\rho}$ and \mathbf{v}_c is in the same direction as \mathbf{v}_g . Thus, the drift velocity cannot remove a particle from the flux surface.

However, actual flux ropes are curved (see Figure 1), leading to an additional curvature drift out of the plane of the loop. In the absence of field line winding, this curvature drift would allow energetic particles to rapidly escape.

Thus, we might consider a toroidal flux rope, in which the cylinder is curved so the loop axis forms a circle. When the field lines wind around the loop axis, the particle orbits along the field lines experience a curvature drift that is sometimes inward and sometimes outward, leading to trapping of a large portion of the drift orbits. This trapping effect is exploited in tokamak devices for plasma confinement for controlled nuclear fusion (Boyd & Sanderson 2003), and we shall refer to it as the “tokamak effect.”

A key motivation for the present work is to explore to what extent the tokamak effect influences the escape of SEPs and the entrance and exit of GCRs from interplanetary magnetic flux ropes (see Ruffolo et al. 2006). However, we cannot directly make use of results for toroidal flux ropes (tokamaks), in part because the winding rate of the flux rope is likely to be non-uniform (Vandas et al. 2002), and also in part because of the convergence of field lines toward the Sun.

The convergence of field lines toward the Sun suggests another idealized configuration: a conical flux rope. The analog to the axial field in the above flux rope models is a radial field spreading out from the Sun, to which an azimuthal (winding) field is added. Compared with the cylindrical flux rope, in which the drift velocity is along the flux surface, for a conical flux rope the vectors ∇B and \mathbf{R}_c are no longer perpendicular to the flux surface and the drift velocity has an outward or inward component, depending on the direction of the winding field.

We can see that interplanetary flux ropes combine features of toroidal flux ropes and conical flux ropes, as indicated in Figure 2. Based on the approximately conical configuration near the Sun, we might expect the net drift to be outward along one leg of the loop and inward along the other, and it is not clear whether the tokamak effect will still trap the drift orbits when the toroidal flux rope is modified in this way. To clarify these multiple effects, in the present work we develop a global analytic model of the magnetic fields of an interplanetary flux rope.

2.2. Basic Requirements for Realistic Drift Orbits

In order to obtain realistic drift orbits, we identify the following desirable requirements for a global, analytic model of an interplanetary magnetic flux rope.

1. The magnetic field must remain divergence-free throughout the flux rope.
2. The magnetic field lines are less twisted close to the Sun (Marubashi 1997). Even if the pre-eruption coronal flux rope were twisted roughly uniformly, there is likely to be stronger stretching of the magnetic cloud along its legs than along its forward portion, tending to yield a lower twist along the legs of the flux rope.
3. Close to the Sun, the magnetic field lines are nearly radial, so the field is directed toward or away from the Sun and its magnitude varies as the distance squared. This is a basic requirement near the Sun where the solar wind expands radially and the magnetic field lines are not strongly twisted. As a result, the flux rope has a wider cross section farther from the Sun.

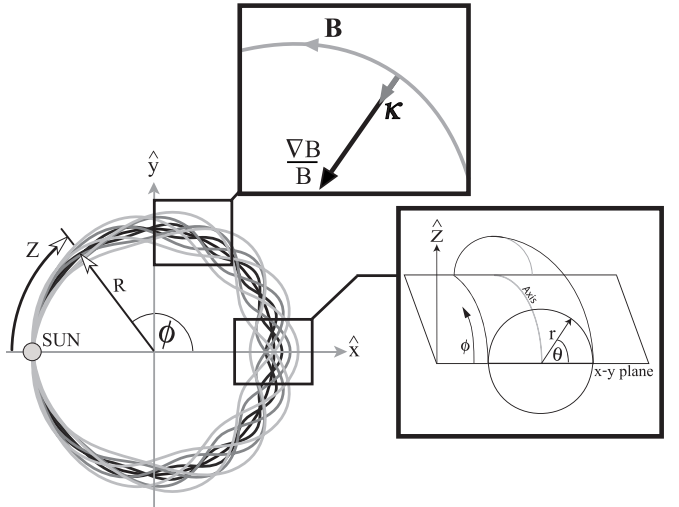


Figure 2. Global analytic magnetic flux rope model developed in this work. We use quasi-toroidal coordinates relative to a circle of radius R , corresponding to the axis of the flux rope: r is the distance from the axis, ϕ is the angle along the axis, and θ is the angle in a cross-sectional plane. The Sun is along the axis at $\phi = \pm\pi$. Each magnetic field line winds around a flux surface of radius $r = a \cos(\phi/2)$, with a nearly radial magnetic field near the Sun. Here, a is the radius of the flux surface at the apex of the loop ($\phi = 0$). The winding rate goes as $\cos(\phi/2)$, so the field lines have less winding (more stretching) near the Sun, and the winding decreases for outer flux surfaces as e^{-a/a_0} . The winding number w is the maximum number of times a field line rotates in θ along the entire flux rope. The field lines shown here are for $w = 10$. For a sample location on a field line, we indicate the relative gradient $(\nabla B)/B$ and curvature κ , which are used in the calculation of the drift velocities.

4. The flux rope has a circular cross section. This is not completely realistic; MHD simulations show that flux ropes are flattened in the radial direction due to the interaction with the solar wind (Vandas et al. 1996, 2002; Manchester et al. 2004). Nevertheless, the assumption of a circular cross section is common and is a useful simplification for the purposes of this initial study of drift orbits. Furthermore, our key results concerning SEPs and GCRs are averaged over the poloidal angle, reducing the importance of the precise geometry as a function of this angle.
5. The magnetic field components as a function of distance from the flux rope axis should be realistic.

We presume that the dynamics of the magnetic field are strongly affected by the motion and expansion of the CME, and therefore do not require a magnetic force-free equilibrium. However, for the timescale of the motion of high-energy particles over the length of the flux rope, we can neglect the time dependence of the large-scale magnetic field.

3. GLOBAL FLUX ROPE MODEL AND DRIFT VELOCITY

To satisfy the requirements in Section 2.2, we have developed a new, global analytic model of magnetic fields in a flux rope. We have chosen to use quasi-toroidal coordinates (r, ϕ, θ) ; Mercier 1962; Sy 1981) as illustrated in Figure 2. These are related to the Cartesian coordinates by

$$x = (R + r \cos \theta) \cos \phi, \quad (4)$$

$$y = (R + r \cos \theta) \sin \phi, \quad (5)$$

$$z = r \sin \theta, \quad (6)$$

where $\phi \in [-\pi, \pi]$, $\theta \in [0, 2\pi]$, and $r \in [0, \infty)$. The metric elements are $(h_r, h_\phi, h_\theta) = (1, R + r \cos \theta, r)$. The axis of the flux rope, at $r = 0$, is a circle of radius R , with the Sun located at $\phi = \pm\pi$. A drawback of this model is that the two legs of the loop approach the Sun from opposite directions, whereas the angle between the two legs would be substantially smaller for an actual CME flux rope. In other words, the shape of a CME flux rope axis is more like a teardrop (Marubashi 1997; Vandas et al. 2002). In any case, we believe that the conclusions of this work are not very sensitive to the shape of the loop axis, and we use a circular shape (see Figure 2) in order to develop an analytic model with the relatively straightforward quasi-toroidal coordinates. We generally use $R = 0.5$ AU so that the distance from the Sun to the loop apex ($\phi = 0$) is 1 AU.

Next, we define the flux surfaces and magnetic field lines according to our requirements. In order to obtain radial magnetic field lines near the Sun, the flux surfaces should have $r \rightarrow 0$ as $\phi \rightarrow \pm\pi$. Thus, we define flux surfaces of circular cross section by

$$r = a \cos(\phi/2), \quad (7)$$

where a represents the maximum radius of the flux surface (at the loop apex, $\phi = 0$). We allow a to vary from zero at the loop axis to a_m at the outer surface of the flux rope, and we generally set a_m to 0.1 AU. To define individual field lines, we specify $\theta(\phi)$ by

$$\theta = w\pi e^{-a/a_0} \sin(\phi/2) + \theta_0. \quad (8)$$

The factor of $\sin(\phi/2)$ ensures that the winding as a function of ϕ is slow (θ is nearly constant) near $\phi = \pm\pi$ and is faster elsewhere, as required in Section 2. The exponential factor provides a more realistic radial dependence, as will be discussed shortly. Then, w is the winding number, representing the total number of complete circuits in θ over the entire flux rope for a close to zero. For general a , the number of complete circuits is $w e^{-a/a_0}$. Now $r(\phi)$ and $\theta(\phi)$ define a field line labeled by a and θ_0 .

Our formulation allows w to be positive or negative, which defines the sense of the winding. When our w value is positive, the flux rope is classified as an “anti-parallel” or “left-handed” type (i.e., when the fingers of your left hand follow B_θ , your left thumb indicates the sign of B_ϕ ; Marubashi 2002). The sign of w also defines the sign of the magnetic helicity (see, e.g., Dasso et al. 2003), and in our case a positive w implies a negative helicity.

The above specification of the field lines then constrains the magnetic field components. Since the field line vector is parallel to the magnetic field vector, the field line trajectory is related to field components by

$$\frac{dr}{B_r} = \frac{rd\theta}{B_\theta} = \frac{(R + r \cos \theta)d\phi}{B_\phi}, \quad (9)$$

$$B_r = \frac{B_\phi}{R + r \cos \theta} \frac{dr}{d\phi}, \quad (10)$$

$$B_\theta = \frac{r B_\phi}{R + r \cos \theta} \frac{d\theta}{d\phi}, \quad (11)$$

where the derivatives are evaluated along a field line, i.e., at constant a and θ_0 .

We are still free to specify the radial dependence of the axial magnetic field, B_ϕ . Observations of interplanetary magnetic clouds typically indicate that the magnetic field is more intense toward the loop axis, and does not tend to zero at the flux rope

boundary. Motivated by the form of Gold & Hoyle (1960) with $B_\phi = B_0/(1 + b^2 r^2)$, we use

$$B_\phi = \frac{B_0}{(a^2/a_0^2 + 1)^{3/2}} \frac{1}{\cos^2(\phi/2)}, \quad (12)$$

where we set $B_0 = 15$ nT and $a_0 = 0.07$ AU. Here, B_0 represents the field along the axis at the loop apex. Our choice of B_0 is based on the estimates of ~ 13.8 – 15.9 nT for the well-known interplanetary flux rope of 1995 October 18–19 (Dasso et al. 2005). We also set the flux rope boundary at $a = 0.1$ AU, which is within the ranges of flux rope radii from surveys of Lepping et al. (1990), who found 0.14 ± 0.05 AU, and Zhao et al. (2001), who found 0.11 ± 0.05 AU. Note that along a field line, B_ϕ must be inversely proportional to the r - θ area of a set of neighboring field lines. In our model, for small, fixed ranges of a and θ_0 that area varies as $\cos^2(\phi/2)$, hence the factor of $1/\cos^2(\phi/2)$ in Equation (12).

In Figure 3, we compare our field components as a function of r with those of three previous models with nonlinear functional dependences (Lundquist 1950; Gold & Hoyle 1960; Krall & Chen 2005), which treated the flux rope as cylindrical. To better compare the functional dependences, in each case we choose parameters so that $B_\phi(r = 0) = 15$ nT and the fields decrease over ~ 0.1 AU. Specifically, for the model of Lundquist (1950) we set the flux rope boundary to 0.1 AU, and for that of Gold & Hoyle (1960) we use $b = 22$ AU $^{-1}$. These two models have been successfully used to fit observational data (e.g., Dasso et al. 2005). We also consider the model of Krall & Chen (2005) as in their Equations (15) and (16), with $a = 0.1$ AU and with the field amplitudes scaled to give $B_\phi(r = 0) = 15$ nT. At the apex, where $\phi = 0$ and $r = a$, our model for B_ϕ is reasonably consistent with previous models up to our flux rope boundary at $r = 0.1$ AU (see Figure 3(a)).

Using Equations (7), (8), and (12), we obtain each magnetic field component in quasi-toroidal coordinates:

$$B_r = -\frac{B_0}{2} \frac{\sin(\phi/2)}{[r^2/a_0^2 + \cos^2(\phi/2)]^{3/2}} \frac{r}{(R + r \cos \theta)}, \quad (13)$$

$$B_\phi = B_0 \frac{\cos(\phi/2)}{[r^2/a_0^2 + \cos^2(\phi/2)]^{3/2}}, \quad (14)$$

$$B_\theta = w B_0 \frac{\pi}{2} \frac{\cos^2(\phi/2)}{[r^2/a_0^2 + \cos^2(\phi/2)]^{3/2}} \frac{r}{(R + r \cos \theta)} e^{-r/[a_0 \cos(\phi/2)]}. \quad (15)$$

The divergence of \mathbf{B} is zero by construction.

In Figures 3(b) and (c), we also compare the poloidal field and total field from previous models with those of our model at the loop apex (where $B_r = 0$). Considering our model for varying winding number (solid lines), we conclude that $w = 10$ is reasonably consistent with previous models. In any case, we will also consider some implications of varying the winding number w .

Given our analytic magnetic field model, we proceed to consider the drift velocity of an energetic particle using Equations (1) and (2). Figure 4 shows the combined (gradient plus curvature) drift velocity components for our magnetic field model with $w = 10$. Here, we consider protons of kinetic energy $E = 1$ GeV ($v = 0.875c$) and pitch angle 45° for a pitch-angle cosine $\mu = 1/\sqrt{2}$. Drift velocity values for other

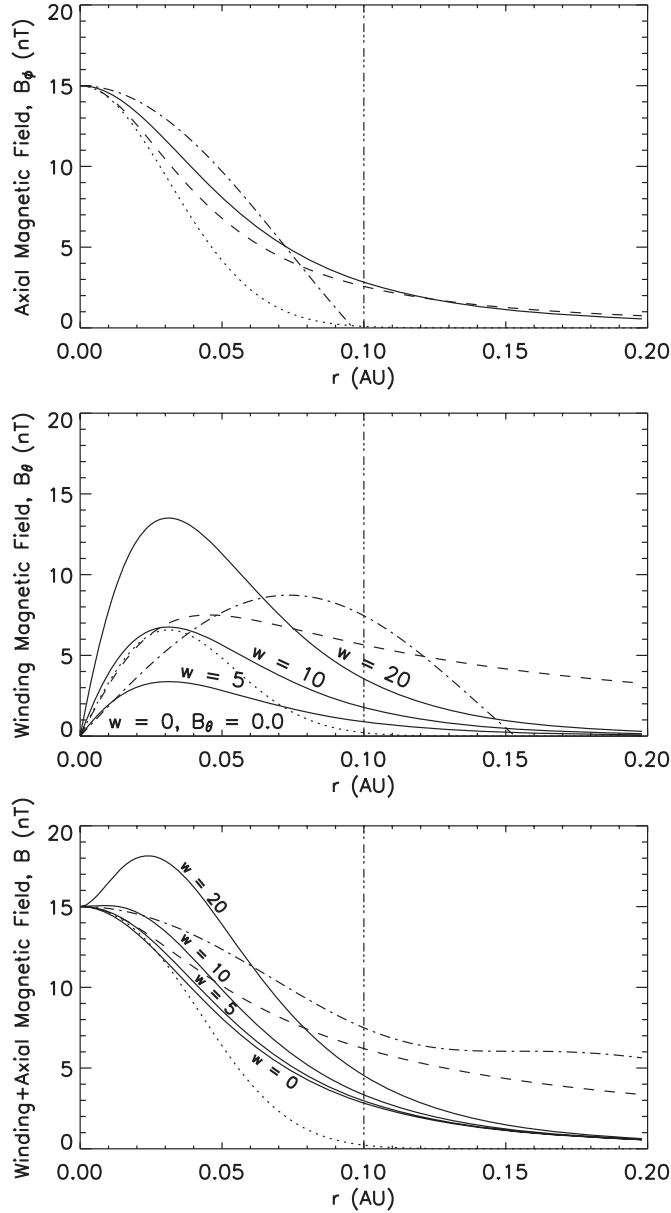


Figure 3. Radial dependence of the magnetic field in our flux rope model for varying winding number w at the loop apex (solid lines), in comparison with previous analytic models of cylindrical flux ropes: Gold & Hoyle (1960; dashed lines), Lundquist (1950; dash-dotted lines), and Krall & Chen (2005; dotted lines). Here, $w = 10$ provides a reasonable agreement with the previous models. In our model, the flux surface parameter a has a maximum value of $a_m = 0.1$ AU, corresponding to $r = 0.1$ AU at the loop apex (vertical lines).

particle species and speeds can be inferred using the scaling from Equations (1) and (2).

Several features of the drift velocity components in Figure 4 are consistent with the general considerations in Section 2. The v_r component is generally smaller in magnitude than the other components (note the expanded scale for v_r in Figure 4); this component would be zero for a cylindrical flux rope. All drift velocity components are much weaker near the Sun (e.g., at $\phi = 0.9\pi$; see short-dashed lines in Figure 4) than at other locations. This is because the magnetic field increases as field lines converge toward the Sun. While v_ϕ and v_θ do not vary strongly with θ , v_r has both positive and negative values, and is strongest at θ for which $\hat{\mathbf{r}}$ is nearly normal to the plane of the flux rope axis. This is due to the curvature drift associated

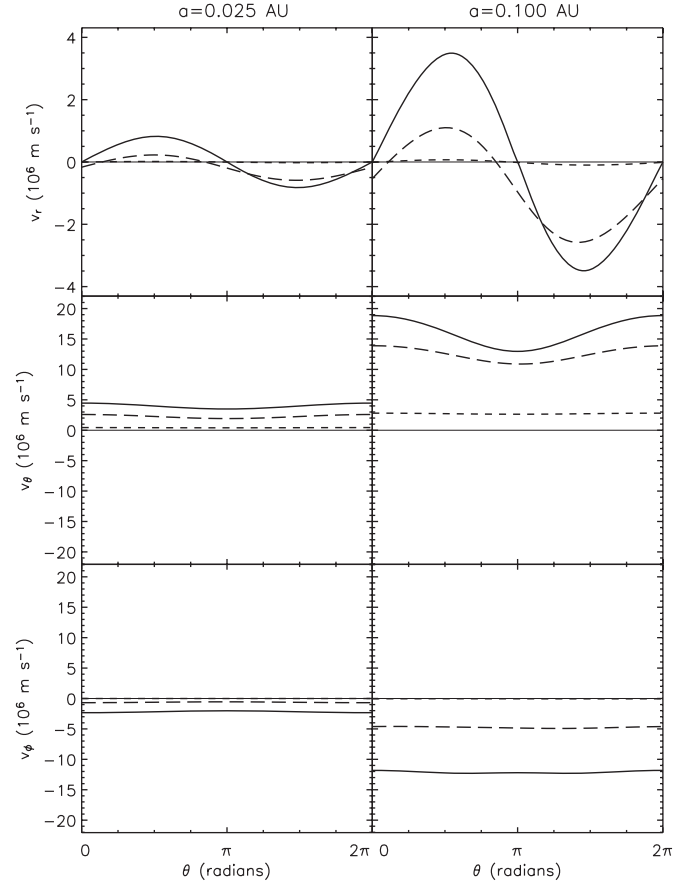


Figure 4. Total gradient and curvature drift velocity of energetic particles in a flux rope as a function of θ along the flux surfaces at $a = 0.025$ AU (left panels) and $a = 0.1$ AU (right panels) at $\phi = 0$ (the loop apex, solid lines), $\phi = 0.5\pi$ (long-dashed lines), and $\phi = 0.9\pi$ (near the Sun, short-dashed lines). Here, we use $w = 10$ and protons of kinetic energy $E = 1$ GeV ($v = 0.875c$), for a pitch angle of 45° ($\mu = 1/\sqrt{2}$). The drift velocity is dominated by θ - and ϕ -components; note the expanded scale used for v_r .

with the large-scale curvature of the loop axis. As the field lines twist along different values of θ , the particle experiences both positive and negative v_r . This is the tokamak effect, which leads to the trapping of drift orbits (Boyd & Sanderson 2003). For $\phi = 0.5\pi$, one can see a substantial imbalance, with a larger range of θ with negative v_r . Such an imbalance is consistent with our expectations for an approximately conical flux rope in which the field lines expand with distance along the loop axis (see Section 2.1). Because these features are all consistent with general considerations, we expect that they are not peculiar to our analytic model, and should apply to any realistic interplanetary magnetic flux rope configuration.

There are numerous symmetries regarding the magnetic fields and drifts in our model. From Equations (1) and (2), we see that the drift velocity is invariant under $\mu \rightarrow -\mu$. When $B_0 \rightarrow -B_0$, reversing the field direction, the drift velocity is also reversed.

In our model, like most analytic and numerical models, the magnetic flux surfaces are invariant under a reflection across the x - y plane (the plane of the loop axis), corresponding to $\theta \rightarrow -\theta$. In general, a field line defined by Equations (7) and (8) is then transformed into a different field line with $w \rightarrow -w$ and $\theta_0 \rightarrow -\theta_0$. Therefore, this reflection symmetry provides us information about the effect of changing w in the model.

To consider the effect of this reflection on vector fields, we apply $\theta \rightarrow -\theta$ and $w \rightarrow -w$, and find that B_r and B_ϕ remain the same, while the poloidal component B_θ changes to $-B_\theta$

(note further that all three magnetic field components are even functions of θ) and the drift velocity components (which are not even functions of θ) transform as $v_r \rightarrow -v_r$, $v_\phi \rightarrow -v_\phi$, and $v_\theta \rightarrow v_\theta$.

The flux surfaces in our model are also invariant under a reflection across the x - z plane, corresponding to $\phi \rightarrow -\phi$. (Note, however, that this does not apply to actual interplanetary flux ropes, because there are asymmetric forces in the interplanetary medium; see Marubashi 1997; Vandas et al. 2002.) According to Equations (7) and (8), each field line is transformed to a field line with $w \rightarrow -w$ (but the same θ_0). The direction of the toroidal field also changes under this transformation, with $B_0 \rightarrow -B_0$. Upon reversing ϕ , w , and B_0 , Equation (12) tells us that $B_\phi \rightarrow -B_\phi$, and from Equations (10) and (11) we see that B_r and B_θ are unchanged. Then, the drift velocity components transform as $v_r \rightarrow -v_r$, $v_\phi \rightarrow v_\phi$, and $v_\theta \rightarrow -v_\theta$.

Finally, it is useful to consider the combination of those two reflection operations followed by $B_0 \rightarrow -B_0$, resulting in $\phi \rightarrow -\phi$ and $\theta \rightarrow -\theta$ for fixed w and B_0 . In other words, this combined operation maps a field line onto itself. The two reflections are equivalent to rotating by 180° about the x -axis, and the θ - and ϕ -components of vector fields are reversed. Then, after taking $B_0 \rightarrow -B_0$, those components are unchanged and the r -component is reversed. We obtain

$$\begin{aligned} B_r(r, \phi, \theta) &= -B_r(r, -\phi, -\theta) \\ B_\phi(r, \phi, \theta) &= B_\phi(r, -\phi, -\theta) \\ B_\theta(r, \phi, \theta) &= B_\theta(r, -\phi, -\theta) \end{aligned} \quad (16)$$

and

$$\begin{aligned} v_r(r, \phi, \theta) &= -v_r(r, -\phi, -\theta) \\ v_\phi(r, \phi, \theta) &= v_\phi(r, -\phi, -\theta) \\ v_\theta(r, \phi, \theta) &= v_\theta(r, -\phi, -\theta) \end{aligned} \quad (17)$$

for fixed field parameters w and B_0 . Thus, in Figure 4 we show results only for $\phi \geq 0$, and results for negative ϕ can be inferred from these symmetry relations.

In the following sections, we examine the implications of the drift velocities for the escape of SEPs from the interior of a flux rope, and the inflow and outflow of GCRs at the flux rope surface.

4. DRIFT ORBITS OF SOLAR ENERGETIC PARTICLES

Now let us consider the drift orbits of energetic particles, such as SEPs, in the interior of a flux rope, and what conditions are necessary for their trapping due to the tokamak effect. For this initial study of the properties of drift orbits, we employ the simplifying assumptions of our global, analytic model, as well as the assumption of a fixed interplanetary magnetic flux rope. Later in this section, we will address the extent to which our results would be affected by the expansion of actual flux ropes, and other physical effects that are not accounted for by the drift orbits.

Here, we concentrate on relativistic solar particles of energy 1 GeV. As discussed in Section 1, such particles are typically injected over short timescales, potentially allowing the determination of an escape time (i.e., the duration of trapping). For the GLE of 2003 October 28, associated with the well-known “Halloween” geomagnetic storm, the relativistic solar proton flux remained elevated and nearly isotropic for 19 hr, which may be associated with propagation inside a closed magnetic flux rope (Bieber et al. 2005; Miroshnichenko et al. 2005; Sáiz et al. 2008). For the GLE of 1989 October 22, Ruffolo et al. (2006)

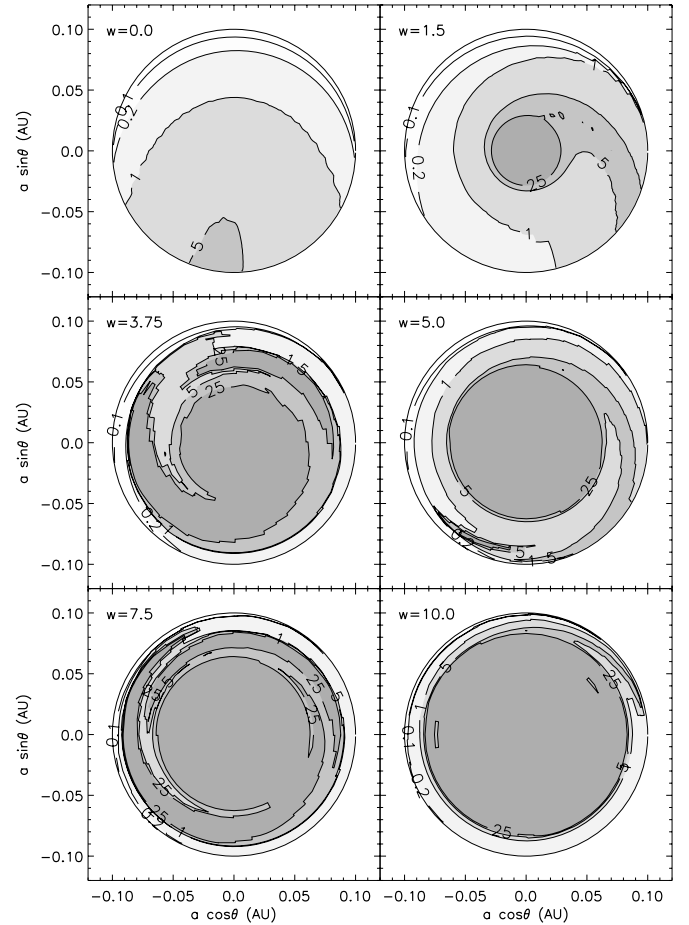


Figure 5. Contour plots of trapping time in hr for drift orbits over 25 hr of solar energetic particles injected at $Z = 0.1$ AU from the Sun along one leg of the loop as a function of the initial position for varying winding number, w . For no winding ($w = 0$), the particles readily escape. For $w \geq 1.5$, drift orbits in the inner portion of the flux rope are trapped for an extended time (as in tokamak experiments for controlled nuclear fusion). There is also a resonance effect: when w is close to an integral multiple of 3.75, some drift orbits from deep inside the loop can escape quickly. When drift orbits remain trapped for tens of hours, other effects can cause particles to escape more quickly (see the text for details).

found clear evidence for propagation in a closed magnetic loop, and the observed SEP density decayed exponentially with an escape time of 3 hr. We note that in addition to the drift orbit motion, i.e., the systematic guiding center motion, SEPs are also subject to the stochastic processes of pitch-angle scattering and perpendicular diffusion, which tend to make the particles escape faster. Thus, the drift orbits must be trapped for at least as long as the observed particle density decay time, i.e., for several hours in some cases. In other words, trapping of drift orbits is a necessary but not sufficient condition for the trapping of actual particle orbits.

Using the model presented in Section 3, we trace the drift orbits of particles, i.e., the motion of the guiding center subject only to the large-scale magnetic field, with results as shown in Figure 5. We use standard approximations that the guiding center moves along the field subject to conservation of the first adiabatic invariant, and perpendicular to the field subject to gradient and curvature drifts. Then, the guiding center location \mathbf{r} evolves according to

$$\frac{d\mathbf{r}}{dt} = \mu v \hat{\mathbf{b}} + \mathbf{v}_g + \mathbf{v}_c, \quad (18)$$

where the drift velocities \mathbf{v}_g and \mathbf{v}_c are calculated from Equations (1) and (2). Note that the velocity of the particle parallel to the field is v times the pitch-angle cosine μ , so the sign of μ determines the direction of motion along the field line. Then, μ at each location is determined by conservation of the first adiabatic invariant, i.e., the magnetic moment M

$$M = \frac{(1 - \mu^2)p^2}{2mqB}, \quad (19)$$

where p is the particle momentum. (Note that for our assumption of a static magnetic field, v and p are constants of the motion because the magnetic force is perpendicular to \mathbf{v} and does not work on the particle.) Figure 6(a) shows how μ varies with $Z = R(\pi - \phi)$, the distance from the Sun along the flux rope, for some sample trajectories. Equation (19) can be rewritten to obtain

$$\mu = \pm \sqrt{1 - \frac{B(\mathbf{r})}{B_T}}, \quad (20)$$

where $B_T = p^2/(2mqM)$ is the magnetic field strength at the turning point (also called a “mirror point”) where μ goes through zero and changes sign, and the particle is reflected.

This well-known process of systematic pitch-angle changes along with changes in magnetic field strength is known as adiabatic focusing or magnetic mirroring. In the absence of drifts, the particle guiding center motion according to Equation (18) would simply bounce from one mirror point to the other at opposing sides of the loop (Figure 6(a)).

Our purpose in solving Equation (18) numerically is to determine how the gradient and curvature drifts affect such guiding center orbits, including whether or for how long they remain trapped within the loop, given the assumption of a fixed loop. We use a fourth-order Runge–Kutta method over most of the orbit. We use a special treatment very close to a turning point. Here, we assume a linear variation in B with distance along the field line, use an analytic formula to estimate the time duration for μ to reverse, and displace the orbit by the drift velocity times that time duration.

To examine the drift orbits of a beam of SEPs, we trace particles from starting locations at $Z = 0.1$ AU. We set $B_0 = 15$ nT for a magnetic field directed counterclockwise along the loop axis in Figure 2. Then, we choose an initial value of $\mu = -0.99$ (with a negative sign for motion away from the Sun with decreasing ϕ and increasing Z) in light of the beam-like distribution of SEPs near the Sun. Due to the rapidly changing magnetic field near the Sun, adiabatic focusing is strong and we can assume that SEPs are concentrated at $|\mu| \approx 1$, even in the presence of pitch-angle scattering (Ruffolo & Khumlumlert 1995).

Figure 5 shows contour plots of the trapping time in hours for drift orbits as a function of the initial position within the circular cross section of the loop. This initial position is specified by the coordinates $a \cos \theta$ and $a \sin \theta$, where a specifies the flux surface in terms of its radius r at the loop apex. The shading indicates the duration over which the drift orbit from that initial position remained within the flux rope. Figure 5 shows contours up to 25 hr. We also traced drift orbits for 50 hr, but the 50 hr contours are almost identical to the 25 hr contours and are not shown for clarity of presentation. In other words, the orbits trapped for 25 hr were almost always trapped for 50 hr as well. Note that these results are for protons of 1 GeV; additional simulations verify that for lower particle speeds, there are slower drifts and longer trapping times.

Figure 5 shows results for varying winding number w , which is the total number of complete circuits in θ over the entire flux rope for field lines near the loop axis. We find that the results in Figure 5 are merely rotated or reflected when reversing B_0 and/or w .

When there is no winding of the field lines ($w = 0$), the particles readily escape due to the overall curvature drift out of the plane of the loop, toward increasing $a \sin \theta$. Thus, the initial locations with the longest trapping times of over 5 hr are near the minimum values of $a \sin \theta$. However, for $w \geq 1.5$ the tokamak effect is clearly in evidence, as the drift orbits that start near the center of the loop are trapped for the duration of the simulation (50 hr). This corresponds to winding of the field lines by as few as 1.5 circuits in θ over the entire flux rope. It is noteworthy that the tokamak effect can trap a fraction of the drift orbits, even though we consider the winding to be reduced near the Sun. Roughly speaking, for greater winding w , a larger fraction of the drift orbits is trapped.

Interestingly, the trapping behavior does not vary monotonically as a function of w . There is a resonance effect: when w is close to an integral multiple of 3.75, some drift orbits from deep inside the loop can escape quickly, and some orbits near the outer edge of the loop remain trapped. Figure 5 shows this for $w = 3.75$ and 7.5. Based on this, we expected and found similar behavior at $w = 11.25$ and 15. For values of w away from the resonance, the trapping behavior is more mundane: orbits that start near the center of the loop are trapped and almost all orbits that start near the outer edge escape quickly.

To understand this behavior, we note that the effect of guiding center drifts on the escape or trapping of drift orbits is related to the r -drift (outward or inward) integrated over the helical field line trajectory as the drift orbit bounces from one leg of the loop to the other and back. For non-resonant values of w , we find that the tokamak effect applies as the outward and inward drifts effectively cancel. For the resonant values of w , the drifts over different parts of the orbit are imbalanced and the net drift is predominantly outward for some starting values of a and θ and predominantly inward for others.

To consider the implications of these results for SEP transport, we note that the key result of Figure 5 is that most drift orbits are in one of two categories: (1) rapidly escaping from the loop, over $\lesssim 5$ hr; or (2) trapped for long times, $\gtrsim 25$ hr. Only a very small fraction of the orbits have trapping durations between 5 and 25 hr. For SEPs with drift orbits in Category 1 (for $|w| \lesssim 1.5$, or the outer portion of a loop with higher $|w|$), we expect that drifts will serve as the dominant mechanism for particles to escape from the loop. For SEPs with drift orbits in Category 2 (found in the inner portion of a loop with $|w| \gtrsim 1.5$), the drifts alone do not allow particles to escape from the loop over 25 hr or longer. Over such a long timescale, other effects such as perpendicular diffusion can no longer be neglected and indeed are likely to cause the particles to escape from the inner portion of the loop.

Without field line winding ($w = 0$), we see that the drift processes will rapidly and systematically remove SEPs from the flux rope. With substantial field line winding ($|w| \geq 1.5$), as frequently inferred for actual interplanetary magnetic flux ropes, the drifts should rapidly and systematically remove SEPs from the outer portion of the flux rope but not from the inner portion. This is consistent with observations that trapping of SEPs can occur for extended time periods. Then, SEPs in the inner portion of the flux rope can undergo perpendicular diffusion to the outer portion, where the drifts subsequently contribute to a faster escape. Thus, we expect that the extended

escape times associated with GLE observations are determined by the diffusion out of the inner portion of the flux rope.

Conversely, when there is a higher density of SEPs or GCRs outside the loop, they can readily enter the outer portion of the flux rope by means of drifts. They can then access the inner portion more slowly by means of perpendicular diffusion.

We would expect our general conclusions regarding the categories of drift orbits to be only weakly model dependent, as we have found the tokamak effect to be quite robust, despite our model's reduced winding near the Sun. What are more model dependent are the specific values of w where resonant behavior is found. We take our results to provide an indication that for actual interplanetary magnetic flux ropes, such resonant behavior could take place, implying an irregular boundary between the aforementioned "inner portion" of the flux rope with trapped drift orbits and an "outer portion" where drifts lead to more rapid escape of particles.

Our general conclusions should also be robust with respect to effects of flux rope expansion and pitch-angle scattering. Regarding flux rope expansion, it is important to consider the effect of adiabatic deceleration, which is a systematic decrease in the particle momentum in an expanding plasma, due to the expansion of the distance between mirror points and/or the distance between the magnetic fluctuations that serve as scattering centers. To approximately estimate the effect of adiabatic deceleration on individual particles, let us assume an isotropic particle distribution. Then, we can use the following formula, which applies for non-relativistic or relativistic particles (Parker 1965; Dorman 1965):

$$\frac{\langle \dot{p} \rangle}{p} = -\frac{1}{3} \nabla \cdot \mathbf{v}_p = -\frac{1}{3} \frac{\dot{V}}{V}, \quad (21)$$

where p is the particle momentum in the plasma frame, \mathbf{v}_p is the plasma velocity, and V is the volume of the flux rope. The above formula can be derived kinetically (Ruffolo 1995) or from a thermodynamic argument in which the interaction of the particles with "scattering centers," such as magnetic irregularities, that move with the plasma allows the particles to be treated as an adiabatic, ideal gas with a volume V defined by the plasma expansion. Thus, we have $p \propto V^{-1/3}$.

The effects of adiabatic deceleration can be considered in two ways: how it affects individual particles and the density of particles at a fixed energy. For the former, note that the drift speed v_d for either the gradient drift or the curvature drift has the following dependence:

$$v_d \sim \frac{pv}{qB\ell}, \quad (22)$$

where ℓ is a characteristic length scale, either the inverse fractional gradient or the radius of curvature. For a homologous expansion, B is inversely proportional to the cross-sectional area, so that $B \propto \ell^{-2}$ (Marubashi & Lepping 2007), and Equation (21) implies that $p \propto \ell^{-1}$. Thus, during the course of adiabatic deceleration, we have $v_d \propto v$ for either non-relativistic or relativistic particles.

Therefore, as adiabatic deceleration reduces the particle speed, the drift speed is also reduced, and the timescale of escape could be longer. Marubashi (2002) has estimated the rate of expansion of three flux ropes observed near the Earth, which were found to double in size ℓ over times ranging from 56 to 144 hr. For such long expansion times, our general conclusions concerning the escape of drift orbits from a flux rope are not noticeably affected.

On the other hand, adiabatic deceleration can also affect the density of a particle population in a specific energy range, which directly relates to observations. Because SEP populations typically have steep energy spectra, adiabatic deceleration reduces the SEP density over a timescale that is much shorter than the expansion timescale. Note that this reduction occurs even if the particle orbits are completely confined within the flux rope. For the specific case of the GLE of 1989 October 22, Ruffolo et al. (2006) estimated that adiabatic deceleration should account for a density decline with an exponential timescale of 19 hr. However, for that event the relativistic solar particle density inside the interplanetary flux rope (due to a preceding CME) was found to decrease faster than that, with an exponential timescale of 3 hr, which was therefore attributed to the escape of SEPs from the flux rope. In sum, when drift orbits are trapped for extended times ($\gtrsim 25$ hr), one must bear in mind that adiabatic deceleration will lead to a decrease in the observed particle density in a given energy range, and perpendicular diffusion can also lead to a faster escape of particles from the region of extended drift orbits.

The drift orbits can be viewed as "unperturbed" trajectories that are perturbed by the stochastic effects of magnetic fluctuations, including pitch-angle scattering and perpendicular diffusion. The role of perpendicular diffusion is to transport particles to other parts of the flux rope, and for the portion that is cross-field diffusion, to enter or exit the flux rope. To visualize the role of pitch-angle scattering, we need to first consider the "unperturbed" trajectories in Figure 6(a). This figure shows sample drift orbit trajectories in terms of Z , a coordinate along the flux rope axis, and μ , the pitch-angle cosine, which in turn determines the rate of streaming, $\dot{Z} = -\mu v$. (The minus sign arises from the choice of $B_0 > 0$ and the direction along which Z increases.) Here, μ is seen to vary with position along the flux rope axis in a manner that conserves the first adiabatic invariant M , with reflection (a change in sign of μ) at mirror points on either leg of the loop. The results shown in Figure 5 are for particles starting near the Sun, i.e., traveling along the outermost paths in Figure 6(a). If pitch-angle scattering, say, near the apex moves particles to the inner paths in Figure 6(a), how will that affect the escape times shown in Figure 5?

To answer this, we examined simulation results for drift orbits starting at the apex instead of the Sun, with different values of μ . We found that particles with larger $|\mu|$ escaped more rapidly. Because particles injected near the Sun as in Figure 5 would have $|\mu|$ close to 1 at the loop apex, their perturbation by pitch-angle scattering would increase the escape time. Thus, this perturbation could increase the portion of SEP orbits that is trapped for long times, in comparison with the results for drift orbits as shown in Figure 5.

Finally, one additional caveat about the escape of SEPs from the interior of a flux rope is that there have been reports of open field line regions embedded inside magnetic clouds in association with an inflow of GCRs (e.g., Bothmer et al. 1997; Cane et al. 2001). Such embedded regions of open field lines can "short circuit" the trapping of drift orbits, and the presence or absence of such an escape path inside the magnetic cloud will also contribute to strong event-to-event variability.

5. DRIFT ORBITS OF GALACTIC COSMIC RAYS

In this section, we consider the inflow or outflow of energetic particles across the boundary of an interplanetary magnetic flux rope due to gradient and curvature drifts. This is relevant to understanding the second stage of Forbush decreases in GCRs.

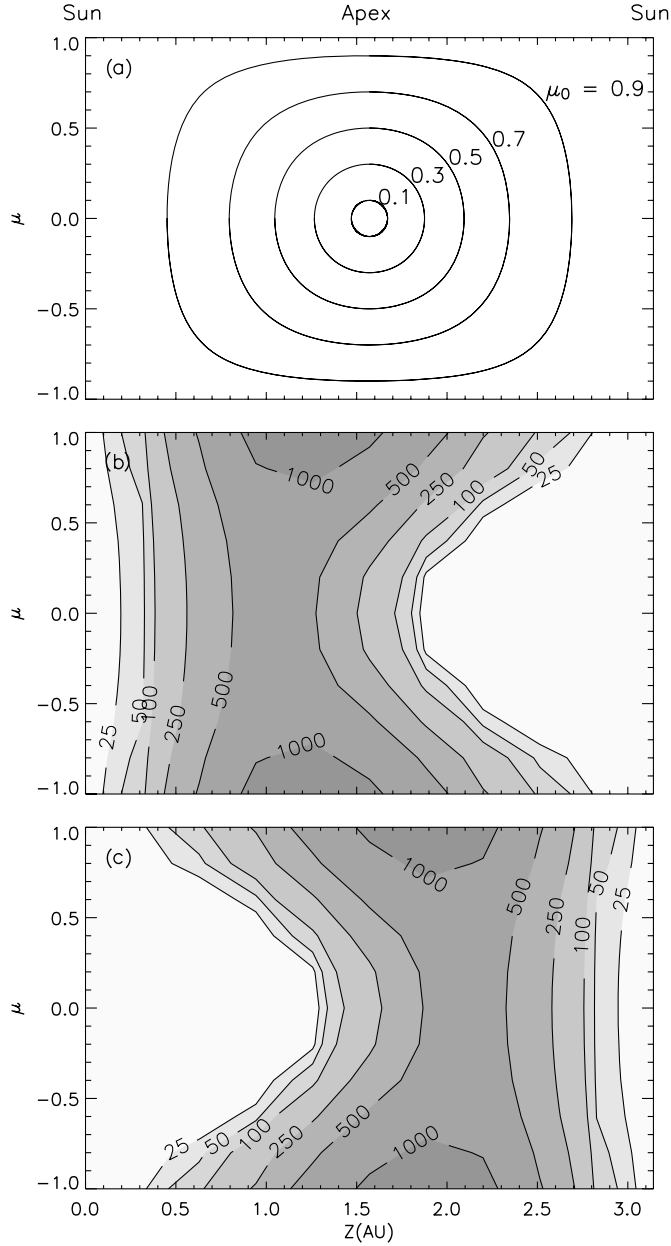


Figure 6. (a) Particle trajectories in terms of μ , the pitch-angle cosine, and Z , the distance from the Sun along the loop, for varying initial values μ_0 at the apex (at $Z = 1.57$ AU). (b) Inflow rate and (c) outflow rate averaged over the surface of the flux rope (i.e., averaged over θ) as a function of μ and Z ; see the text for details. During a Forbush decrease, this implies that Galactic cosmic rays preferentially enter along one leg of the loop and exit along the other, which will contribute to a unidirectional anisotropy and net flow of cosmic rays. The flow direction is determined by the poloidal field direction.

Let us consider the drift velocity outward across the flux rope surface, $v_n = (\mathbf{v}_g + \mathbf{v}_c) \cdot \hat{\mathbf{n}}$, where $\hat{\mathbf{n}}$ is the outward normal to the surface. We find it useful to separately consider regions with inflow and regions with outflow due to drifts.

It is not particularly important to study the position θ along the surface where the particles exit or enter the loop, especially given the helical trajectories of field lines and the large θ -components of guiding center drifts, from which we expect any density non-uniformities to spread rather rapidly in θ . Thus, we integrate over $r_{\max} d\theta$ at the flux rope boundary to determine the overall inflow and outflow at a given distance $Z = R(\pi - \phi)$ from the Sun along the loop axis (recall that we use $R = 0.5$ AU). We

define the outflow rate as

$$\begin{aligned} O(Z) &\equiv r_{\max} \int_0^{2\pi} v_n H(v_n) d\theta \\ &= a_{\max} \cos(\phi/2) \int_0^{2\pi} v_n H(v_n) d\theta, \end{aligned} \quad (23)$$

where H is the Heaviside step function, valued at 1 when its argument is positive and 0 otherwise. The step function H serves to select only values of θ where the outward drift velocity is positive. We evaluate $O(Z)$ in units of AU km s⁻¹ to aid in its interpretation as a drift velocity (in km s⁻¹) integrated over the circumference of the flux rope (in AU). This outflow rate $O(Z)$ is weighted for the surface area (i.e., loop circumference) at each distance Z , which is proportional to $\cos(\phi/2)$. When multiplying $O(Z)$ by a (constant) particle density, one obtains the particles exiting the flux rope per time per distance Z along the loop. Similarly, we define the inflow rate as

$$\begin{aligned} I(Z) &\equiv r_{\max} \int_0^{2\pi} |v_n| H(-v_n) d\theta \\ &= a_{\max} \cos(\phi/2) \int_0^{2\pi} |v_n| H(-v_n) d\theta, \end{aligned} \quad (24)$$

where the step function now selects only values of θ where the drift velocity at the flux surface is inward.

Figures 6(b) and (c) show the inflow and outflow rates, respectively, as a function of μ and Z . The inflow and outflow rates are related by the reflection symmetry around the loop apex. The inflow is predominantly along one leg (at low Z) and the outflow is predominantly along the other (at high Z). We can understand this behavior in terms of the qualitative drift properties discussed in Section 2. At the loop apex, the drift due to the large-scale curvature is out of the loop plane, with a balanced inflow and outflow. In contrast, along the legs of the loop, the approximately conical flux rope has drifts with a systematic inflow along one leg and outflow along the other. There is relatively little inflow or outflow close to the Sun ($Z \approx 0$ or $2\pi R$) because of the stronger magnetic field and lower drift velocity, as well as the lower surface area of the loop.

Let us now consider the implications for the second stage of Forbush decreases, in which there is a relative paucity of GCR inside the loop (e.g., because the loop overexpands in comparison with the solar wind) for an observed density decrease of up to $\sim 25\%$ (Cane et al. 1996). There is also a net inflow of particles from the denser population outside, without which the second-stage Forbush decrease would have a much larger magnitude. When interpreting our results for the inflow and outflow rates, we must consider whether the particle density can realistically be considered to be nearly constant as a function of Z . In interplanetary space, a fast CME drives a shock, which extends farther in longitude than the flux rope (Cane 2000). The so-called sheath region between the shock and the flux rope is not normal solar wind, and indeed has a substantially different geometry near the two legs of the flux rope. Nevertheless, in a multispacecraft study by Cane et al. (1994), there was a remarkable example (due to a solar event on 1978 March 6) where three spacecraft observed a Forbush decrease at the apex and at either side, and it was found that the GCR density just before the second stage (i.e., just before the spacecraft entered the loop) was quite similar at all three locations. This is evidence that the GCR density in the sheath

region can be considered approximately constant as a function of Z .

As discussed in Section 1, we expect drifts to play a significant role in the transport of energetic particles across the boundary of the flux rope. Our result implies that drifts should contribute to a flow of GCRs in one direction along the loop, as more particles enter the loop along one leg and exit along the other, as indicated in Figure 1. (The flow follows the $Z-\mu$ trajectories shown in Figure 6(a); note that the choice of $B_0 > 0$ as used Figure 6 implies that particles with positive μ move toward lower Z .) This flow should be observable as a net unidirectional anisotropy during the second stage of a Forbush decrease. When changing the sign of B_0 (changing the magnetic field direction) or w (reversing the handedness or helicity), Figures 6(b) and (c) are switched, i.e., the GCR flow direction is reversed. Thus, we find that the flow direction depends on the sign of the poloidal field B_θ , following the direction of $\nabla \times (B_\theta \hat{\theta})$. In other words, there is a “right-hand rule” between B_θ and the flow direction: if the fingers of your right hand follow B_θ around the loop, your right thumb points along the flow direction.

Note that we would expect a similar flow of SEPs in the case where there is a higher density of SEPs outside the flux rope (see, e.g., Lario et al. 2004). Here, similar physical processes apply, with a decrease in the SEP density inside the flux rope due to adiabatic deceleration that can be filled in by an inflow from outside.

As a reality check for the second-stage Forbush decrease, we consider the time over which the inflow rate $I(Z)$ can fill the flux rope with GCRs. For the interplanetary flux rope on 1989 October 22, Ruffolo et al. (2006) inferred a density decay time of 19 hr due to adiabatic deceleration associated with the loop expansion. If guiding center drifts are indeed largely responsible for the transport of particles into the flux rope, they should fill the rope over a timescale of several hours. A much shorter timescale would allow the GCR density to reach ambient levels, in contradiction with the second-stage Forbush decrease, and a much longer timescale would imply that drifts do not play a significant role in the flow of GCRs into the flux rope.

Based on $I(Z)$ (see Figure 6(b)) averaged over μ and integrated over Z , and considering the total volume of the flux rope, $V = \pi^2 a_{\max}^2 R = 0.05 \text{ AU}^3$, we obtain a filling time of 2.3 hr. Actually, this is a lower limit on the time to fill the flux rope, because according to our computer simulations, drift orbits that enter the flux rope remain near the outer boundary, and a large fraction of them exit again after only a few minutes. Thus, while $I(Z)$ is relevant to the unidirectional anisotropy of GCRs as discussed above, it does not properly represent the inflow of GCRs to the interior of the flux rope. To properly estimate the fraction of GCRs that enter and remain inside the flux rope would require accounting for the stochastic processes of pitch-angle scattering and perpendicular diffusion, which is beyond the scope of the present work. In any case, we see that the filling time due to drifts should be substantially greater than 2.3 hr, which is consistent with the order of magnitude required to account for second-stage Forbush decreases.

6. CONCLUSIONS

1. In order to study the drift orbits of energetic particles in an interplanetary magnetic flux rope, we have found it useful to develop a global, analytic flux rope model satisfying the following requirements.

- a) The magnetic field is divergence free.
- b) The field lines are less twisted close to the Sun.

- c) The field lines are nearly radial close to the Sun.
- d) The flux rope cross section is circular for simplicity.
- e) The magnetic field components as a function of distance from the flux rope axis are realistic.

2. We have determined the guiding center drift velocity throughout the flux rope. It is predominantly along flux surfaces, with a small component outward or inward.

3. For a flux rope with no winding of the magnetic field lines, energetic particles (e.g., SEPs) can rapidly escape from the entire flux rope. With winding of at least 1.5 complete circuits over the flux rope, there is an inner portion of the flux rope where drift orbits are trapped, and an outer portion where they rapidly escape.

4. SEPs can escape from the inner portion of a flux rope with $|w| \geq 1.5$ by means of perpendicular diffusion or embedded open field structures, and drifts can rapidly remove them from the outer portion of the flux rope. Conversely, when there is a higher density of SEPs or GCRs outside the loop, they can readily enter the outer portion of the flux rope by means of drifts, and enter the inner portion by means of diffusion or embedded open field structures.

5. We have found a resonance effect for values of the winding number w close to integral multiples of a certain value, where there is a complex boundary between the inner portion of the flux rope with trapped drift orbits and the outer portion with escaping drift orbits, and some orbits from deep inside can rapidly escape.

6. The drifts across the boundary of the flux rope are predominantly inward along one leg of the loop and predominantly outward along the other.

7. For a second-stage Forbush decrease in GCRs, we expect the guiding center drifts to contribute to a net unidirectional flow (anisotropy) of GCRs in a direction determined by the sign of the poloidal field B_θ . This also applies to situations with a higher density of SEPs outside the loop.

This work was partially supported by a Development and Promotion of Science and Technology Talents (DPST) Project Scholarship and the Thailand Research Fund.

REFERENCES

- Bieber, J. W., Clem, J., Evenson, P., Pyle, R., Ruffolo, D., & Sáiz, A. 2005, *Geophys. Res. Lett.*, 32, L03S02
 Bieber, J. W., Evenson, P., Dröge, W., Pyle, R., Ruffolo, D., Rujiwarodom, M., Toopkrai, P., & Khumlumert, T. 2004, *ApJ*, 601, L103
 Bieber, J. W., et al. 2002, *ApJ*, 567, 622
 Bothmer, V., et al. 1997, Proc. 25th Int. Cosmic Ray Conf. (Durban), 1, 333
 Boyd, T. J. M., & Sanderson, J. J. 2003, *The Physics of Plasmas* (Cambridge: Cambridge Univ. Press)
 Burlaga, L. F. 1995, *Interplanetary Magnetohydrodynamics* (New York: Oxford Univ. Press)
 Burlaga, L. F., Hundhausen, A. J., & Zhao, X.-P. 1981a, *J. Geophys. Res.*, 86, 8893
 Burlaga, L., Sittler, E., Mariani, F., & Schwenn, R. 1981b, *J. Geophys. Res.*, 86, 6673
 Cane, H. V. 2000, *Space Sci. Rev.*, 93, 55
 Cane, H. V., Richardson, I. G., & von Rosenvinge, T. T. 1996, *J. Geophys. Res.*, 101, 21561
 Cane, H. V., Richardson, I. G., von Rosenvinge, T. T., & Wibberenz, G. 1994, *J. Geophys. Res.*, 99, 21429
 Cane, H. V., Richardson, I. G., Wibberenz, G., Dvornikov, V. M., & Sdobnov, V. E. 2001, Proc. 27th Int. Cosmic Ray Conf. (Hamburg), 9, 3531
 Dasso, S., Mandrini, C. H., Démoulin, P., & Farrugia, C. J. 2003, *J. Geophys. Res.*, 108, 1362
 Dasso, S., Mandrini, C. H., Démoulin, P., Luoni, M. L., & Gulisano, A. M. 2005, *Adv. Space Res.*, 35, 711
 Dorman, L. I. 1965, Proc. 9th Int. Cosmic Ray Conf. (London), 1, 292
 Forbush, S. E. 1937, *Phys. Rev.*, 51, 1108

- Forbush, S. E. 1946, *Phys. Rev.*, **70**, 771
- Getmantsev, G. G. 1963, *SvA*, **6**, 477
- Gold, T., & Hoyle, F. 1960, *MNRAS*, **120**, 89
- Gonzalez, W. D., & Tsurutani, B. T. 1987, *Planet. Space Sci.*, **35**, 1101
- Gopalswamy, N., Xie, H., Yashiro, S., & Usoskin, I. 2005, Proc. 29th Int. Cosmic Ray Conf. (Pune), 1, 169
- Gosling, J. T. 1990, in Physics of Magnetic Flux Ropes, ed. C. T. Russell, E. R. Priest, & L. C. Lee (AGU Geophysical Monograph 58; Washington, DC: AGU), 343
- Gosling, J. T., & McComas, D. J. 1987, *Geophys. Res. Lett.*, **14**, 355
- Hess, V. F., & Demmelmair, A. 1937, *Nature*, **140**, 316
- Jokipii, J. R. 1966, *ApJ*, **146**, 480
- Kahler, S. 1994, *ApJ*, **428**, 837
- Kocharov, L., Kovaltsov, G. A., Torsti, J., & Huttunen-Heikinmaa, K. 2005, *J. Geophys. Res.*, **110**, A12S03
- Kocharov, L., Saloniemi, O., Torsti, J., Kovaltsov, G., & Riihonen, E. 2007, *ApJ*, **654**, 1121
- Kóta, J., & Jokipii, J. R. 2000, *ApJ*, **531**, 1067
- Krall, J., & Chen, J. 2005, *ApJ*, **628**, 1046
- Lario, D., Decker, R. B., Roelof, E. C., Reisenfeld, D. B., & Sanderson, T. R. 2004, *J. Geophys. Res.*, **109**, A01107
- Lepping, R. P., Burlaga, L. F., & Jones, J. A. 1990, *J. Geophys. Res.*, **95**, 11957
- Lundquist, S. 1950, *Ark. Fys.*, **2**, 361
- Manchester, W. B., IV, et al. 2004, *J. Geophys. Res.*, **109**, A02107
- Marubashi, K. 1997, in Coronal Mass Ejections, ed. N. Crooker, J. Joselyn, & J. Feynman (AGU Geophysical Monograph 99; Washington, DC: AGU), 147
- Marubashi, K. 2000, *Adv. Space Res.*, **26**, 55
- Marubashi, K. 2002, *J. Comm. Res. Lab.*, **49**, 41
- Marubashi, K., & Lepping, R. P. 2007, *Ann. Geophys.*, **25**, 2453
- Matthaeus, W. H., Qin, G., Bieber, J. W., & Zank, G. 2003, *ApJ*, **590**, L53
- Mercier, C. 1962, *Nucl. Fusion Suppl.*, **2**, 801
- Meyer, P., Parker, E. N., & Simpson, J. A. 1956, *Phys. Rev.*, **104**, 768
- Miroshnichenko, L. I., Klein, K.-L., Trottet, G., Lantos, P., Vashenyuk, E. V., Balabin, Y. V., & Gvozdevsky, B. B. 2005, *J. Geophys. Res.*, **110**, A09S08
- Parker, E. N., *Planet. Space Sci.*, **13**, 9
- Qin, G., Matthaeus, W. H., & Bieber, J. W. 2002, *ApJ*, **578**, L117
- Reames, D. V. 1999, *Space Sci. Rev.*, **90**, 413
- Reames, D. V. 2009, *ApJ*, **693**, 812
- Richardson, I. G., Dvornikov, V. M., Sdobnov, V. E., & Cane, H. V. 2000, *J. Geophys. Res.*, **105**, 12579
- Ruffolo, D. 1995, *ApJ*, **442**, 861
- Ruffolo, D., Chuchai, P., Wongpan, P., Minnie, J., Bieber, J. W., & Matthaeus, W. H. 2008, *ApJ*, **686**, 1231
- Ruffolo, D., & Khumlumlert, T. 1995, *Geophys. Res. Lett.*, **22**, 2073
- Ruffolo, D., Tooprakai, P., Rujitarodom, M., Khumlumlert, T., Wechakama, M., Bieber, J. W., Evenson, P., & Pyle, R. 2006, *ApJ*, **639**, 1186
- Sáiz, A., Ruffolo, D., Bieber, J. W., Evenson, P., & Pyle, R. 2008, *ApJ*, **672**, 650
- Sakharov, A. D. 1961, in Plasma Physics and the Problem of Controlled Thermonuclear Reactions, Vol. 1, ed. M. A. Leontovich (New York: Pergamon), 21
- Sy, W. N.-C. 1981, *J. Phys. A: Math. Gen.*, **14**, 2095
- Tamm, I. E. 1961a, in Plasma Physics and the Problem of Controlled Thermonuclear Reactions, Vol. 1, ed. M. A. Leontovich (New York: Pergamon), 1
- Tamm, I. E. 1961b, in Plasma Physics and the Problem of Controlled Thermonuclear Reactions, Vol. 1, ed. M. A. Leontovich (New York: Pergamon), 35
- Torsti, J., Riihonen, E., & Kocharov, L. 2004, *ApJ*, **600**, L83
- Tousey, R. 1973, *Space Res.*, **13**, 713
- Tranquille, C., Sanderson, T. R., Marsden, R. G., Wenzel, K.-P., & Smith, E. J. 1987, *J. Geophys. Res.*, **92**, 6
- Tylka, A. J., et al. 2003, Proc. 28th Int. Cosmic Ray Conf. (Tsukuba), 3305
- Urch, I. H. 1977, *Ap&SS*, **46**, 389
- Vandas, M., Fischer, S., Dryer, M., Smith, Z., & Detman, T. 1996, *J. Geophys. Res.*, **101**, 2505
- Vandas, M., Odstrčil, D., & Watari, S. 2002, *J. Geophys. Res.*, **107**, 1236
- Wilson, J. W., Goldhagen, P., Rafnsson, V., Clem, J. M., De Angelis, G., & Friedberg, W. 2003, *Adv. Space Res.*, **32**, 3
- Zhao, X. P., Hoeksema, J. T., & Marubashi, K. 2001, *J. Geophys. Res.*, **106**, 15643